Dalton Transactions

PAPER

View Article Online
View Journal | View Issue

Cite this: *Dalton Trans.*, 2017, **46**, 1520

Investigation of a new bis(carboxylate)triazole-based anchoring ligand for dye solar cell chromophore complexes†

Alessandro Sinopoli,[a] Fiona A. Black,[b] Christopher J. Wood,[b] Elizabeth A. Gibson*[b] and Paul I. P. Elliott*[a]

A novel anchoring ligand for dye-sensitised solar cell chromophoric complexes, 1-(2,2′-bipyrid-4-yl)-1,2,3-triazole-4,5-dicarboxylic acid (dctzbpy), is described. The new dye complexes $[Ru(bpy)_2(dctzbpy)][PF_6]_2$ (**AS16**), $[Ir(ppy)_2(dctzbpy)][PF_6]$ (**AS17**) and $[Re(dctzbpy)(CO)_3Cl]$ (**AS18**) were prepared in a two stage procedure with intermediate isolation of their diester analogues, **AS16-Et$_2$**, **AS17-Et$_2$** and **AS18-Et$_2$** respectively. Electrochemical analysis of **AS16-Et$_2$**, **AS17-Et$_2$** and **AS18-Et$_2$** reveal reduction potentials in the range −1.50 to −1.59 V (*vs.* Fc^+/Fc) which are cathodically shifted with respect to that of the model complex $[Ru(bpy)_2(dcbH_2)]^{2+}$ (**1**) (E_{red} = −1.34 V, $dcbH_2$ = 2,2′-bipyridyl-4,4′-dicarboxylic acid). This therefore demonstrates that the LUMO of the complex is correctly positioned for favourable electron transfer into the TiO_2 conduction band upon photoexcitation. The higher energy LUMOs for **AS16** to **AS18** and a larger HOMO–LUMO gap result in blue-shifted absorption spectra and hence reduced light harvesting efficiency relative to their $dcbH_2$ analogues. Preliminary tests on TiO_2 n-type and NiO p-type DSSCs have been carried out. In the cases of the Ir(III) and Re(I) based dyes **AS17** and **AS18** these show inferior performance to their $dcbH_2$ analogues. However, the Ru(II) dye **AS16** (η = 0.61%) exhibits significantly greater efficiency than **1** (η = 0.1%). In a p-type cell **AS16** shows the highest photovoltaic efficiency (η = 0.028%), almost three times that of cells incorporating the benchmark dye coumarin C343.

Received 22nd July 2016,
Accepted 3rd January 2017

DOI: 10.1039/c6dt02905a

rsc.li/dalton

Introduction

The application of transition metal complexes, principally those of ruthenium(II), have attracted enormous attention for their application in n-type dye-sensitised solar cells (DSSC).[1–4] The relatively long-lived triplet metal-to-ligand charge-transfer (^{3}MLCT) states of these complexes[5] allow efficient charge injection into the electrode on which the complex is adsorbed. Innumerable reports have appeared in the literature on the design and modification of the ligand set for these complexes in order to enhance the optical absorption cross-section to increase light harvesting efficiency and to optimise the ground state and excited state oxidation potentials for charge-injection and dye regeneration processes.[6] A critical component of these dye complexes is therefore the ligand on which the ^{3}MLCT state is localised and which anchors the complexes to the electrode. The energy of the lowest-unoccupied molecular orbital (LUMO) of the dye, localised on this ligand then largely determines the excited state oxidation potential which must be correctly positioned relative to the Fermi level of the electrode to favour efficient charge injection, and relative to the electrolyte redox couple to minimise short-circuit reactions. Whilst complexes of ruthenium dominate the literature dyes based on a variety of metals have been evaluated including osmium,[7] platinum,[8] rhenium,[9] iron,[10] and iridium[11] as well as zinc porphyrins.[12] Great strides have also been taken in the optimisation of metal free organic dyes.[13,14]

Over thirty years ago, Goodenough and co-workers[15] reported the use of 4,4′-dicarboxy-2,2′-bipyridine ($dcbH_2$, Fig. 1) as an ambidentate ligand for coordination to Ru(II) and metal oxide semiconductors. Strong electronic coupling between the MLCT excited states of $dcbH_2$-containing Ru compounds and TiO_2 has been inferred from femtosecond transient absorption spectroscopy, and the timescales extracted from such data are on the order of <25 fs.[16] To this day $dcbH_2$ remains the most efficient and widely utilised anchoring ligand for applications in DSSCs, however, a number of other carboxylate-based variant ligands have been investigated. Heuer *et al.* reported the design of a new bipyridine based

[a]*Department of Chemistry, University of Huddersfield, Queensgate, Huddersfield, HD1 3DH, UK. E-mail: p.i.elliott@hud.ac.uk*
[b]*School of Chemistry, Newcastle University, Newcastle upon Tyne, NE1 7RU, UK. E-mail: elizabeth.gibson@ncl.ac.uk*

†Electronic supplementary information (ESI) available. See DOI: 10.1039/c6dt02905a

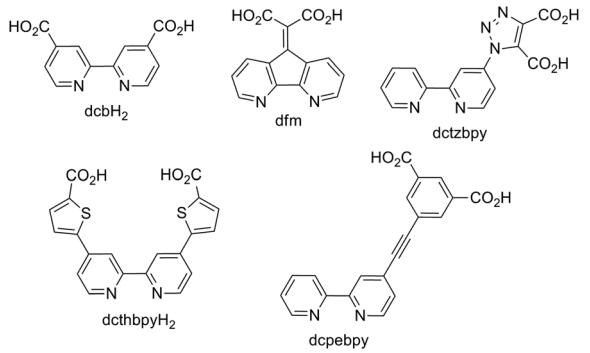

Fig. 1 Structures of selected carboxylate-based DSSC anchoring ligands.

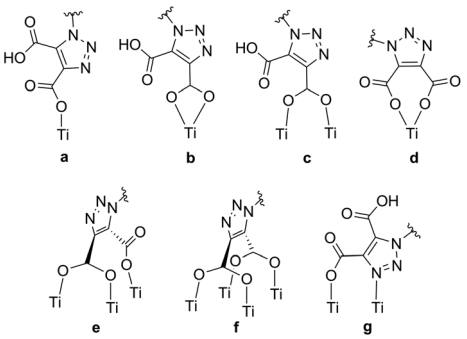

Fig. 2 Selection of the potential TiO_2 anchoring modes that could be adopted by the dctzbpy ligand.

anchoring ligand (4,5-diazafluoren-9-ylidene)malonic acid (dfm, Fig. 1) together with its corresponding complex $[Ru(bpy)_2(dfm)]^{2+}$ (bpy = 2,2′-bipyridyl).[6] Mishra *et al.* prepared the complex **BCT-1**, $[Ru(dcthbpyH)_2(NCS)_2][NBu_4]_2$, where the distance between the bpy core of the ligand and its anchoring carboxylate group has been extended by the introduction of a thiophene spacer ($dcthbpyH_2$).[17] This increases charge separation upon charge injection and reduces the rate of recombination but also leads to augmentation of the light absorption properties over the corresponding $dcbH_2$ complex. This yielded an overall conversion efficiency of 6.1% compared with the 4.8% achieved using the archetypal DSSC dye **N3** ($[Ru(dcbH_2)_2(NCS)_2]$). In an attempt to minimise the rate constant for charge recombination, Abrahamsson *et al.* introduced a phenylenethynylene unit between a bpy ligand and the surface anchoring groups (dcpebpy, Fig. 1), preparing the corresponding $[Ru(dcebpy)(bpy)(NCS)_2]$ complex. This resulted in a recombination rate three times smaller compared to that for **N3**.[18]

Whilst carboxylates represent by far the most commonly encountered anchoring moiety DSSC dyes with other anchoring groups have also been investigated. These include phosphonic acid appended copper(I) and ruthenium(II) complexes[19–21] and also boronic acid derivatised complexes.[22]

In contrast to the wealth of literature on transition metal-based dyes for n-type DSSCs, only a few examples have been reported for NiO p-type cells.[23–30] Pellegrin *et al.* have reported ruthenium(II)-based sensitisers for p-type DSSC devices with phosphonic acid, thiocarboxylate and catechol derived anchoring groups.[29] Ji *et al.* have reported cyclometalated ruthenium complexes of the type $[Ru(N^N)_2(C^N)]^+$ as sensitisers for p-type DSSCs.[28] Addition of a rigid biphenylene spacer between the carboxylate anchor and the aryl ring of the cyclometalated ligand led to a marked increase in device efficiency (0.05% compared to 0.009% with no spacer). Recently Wood *et al.* reported bis(bidentate) ruthenium(II) based dye complexes bearing electron rich carboxylate derivatised triarylamine anchoring groups yielding efficiencies of up to 0.09%.[27] Massin *et al.* have also reported carboxylate-appended triarylamine functionalised dyes with a $[(Ph_2C{=}C{=}Ru(dppe)_2)]$ core (dppe = 1,2-bis(diphenylphosphino)ethane).[25]

Through the use of triazole-based "click" chemistry[31] we report here the design and synthesis of the novel anchoring ligand (2,2′-bipyrid-4-yl)-1,2,3-triazole-4,5-dicarboxylic acid (dctzbpy, Fig. 1). Triazole moieties have been utilised in conjugated polymers and results suggested that the linkage is somewhat electronically insulating.[32,33] Whilst this might be expected to impair to some extent the rate of charge injection into TiO_2 for an immobilised dye, this could significantly retard recombination reactions thereby enhancing overall photovoltaic efficiency. The designed anchor ligand also presents conformational freedom that would enable multiple possibilities for TiO_2 surface coordination modes to be envisaged. For example, the various possibilities for coordination by one carboxylate group (monodentate (**a**), bidentate (**b**) or bridging (**c**) in Fig. 2), both carboxylate groups (bidentate (**d**), tridentate (**e**), tetradentate (**f**)) or anchoring through the 4-position carboxylate with additional surface coordination of the triazole-N3 atom (**g**) could result in highly favourable adsorption characteristics. Further anchoring modes through hydrogen bonding between carboxylic acid and surface oxygen atoms or carboxylate with surface hydroxyl groups can also be envisaged.

We also report the preparation of ruthenium(II), iridium(III) and rhenium(I) complexes **AS16-Et$_2$** to **AS18-Et$_2$** of the initial diethyl ester of the dctzbpy ligand and subsequent photophysical and electrochemical analyses. Further, we report the hydrolysis of these complexes to their corresponding diacids **AS16** to **AS18** (Fig. 3) and pilot studies on their utilisation in DSSC test devices with comparison to corresponding $dcbH_2$ complexes **1** to **3**.

Results & discussion

The above mentioned ligand, dctzbpy, was prepared by the route described in Scheme 1. We, and others, have previously reported the preparation and reactivity of the bpy derivative 4-azido-2,2′-bipyridyl.[34,35] This azide precursor was subject to thermally driven cycloaddition with one equivalent of diethyl acetylenedicarboxylate in refluxing toluene to furnish the diester diethyl-1-(2,2′-bipyrid-4-yl)-1,2,3-triazole-4,5-dicarboxy-

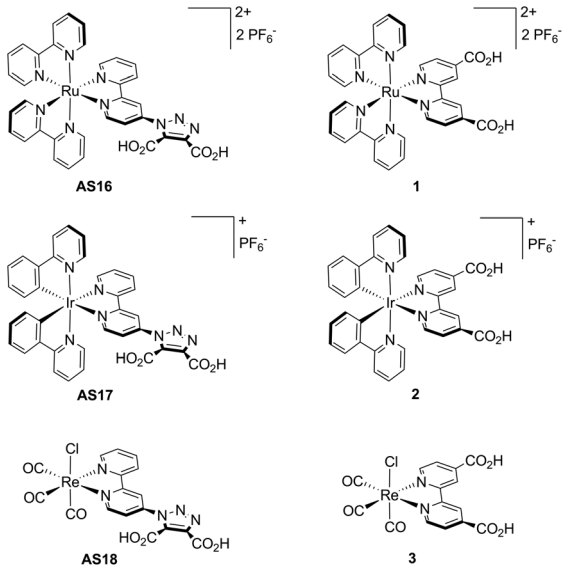

Fig. 3 Structure of complexes **AS16–18** and their $dcbH_2$ analogues **1–3**.

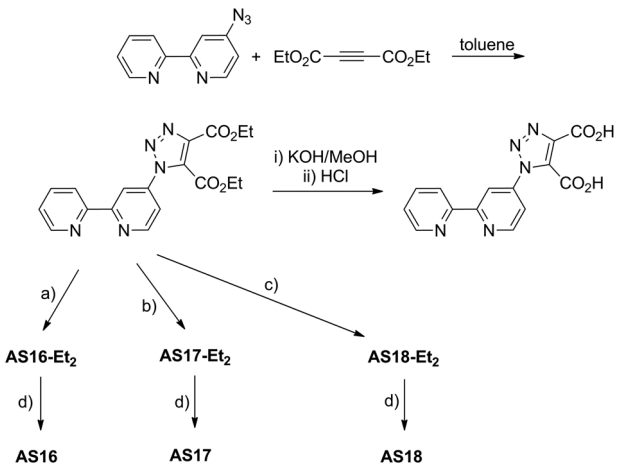

Scheme 1 Synthesis of the target 1-(2,2′-bipyrid-4-yl)-1,2,3-triazole-4,5-dicarboxylic acid ligand and complexes **AS16** to **AS18**: (a) (i) [Ru(bpy)$_2$Cl$_2$], EtOH, reflux, (ii) NH_4PF_6, MeOH; (b) (i) [Ir(ppy)$_2$Cl]$_2$, CH_2Cl_2/MeOH, reflux, (ii) NH_4PF_6, MeOH; (c) [Re(CO)$_5$Cl], toluene, reflux; (d) (i) KOH/acetone, HCl, (ii) NH_4PF_6.

late. Cycloaddition was confirmed by infrared spectroscopy with the disappearance of the azide stretch corresponding to the starting material (2115 cm^{-1}) and the appearance of new CO stretching bands for the carboxylate substituents on the triazole ring (1735 cm^{-1}). The ester groups then underwent hydrolysis to the corresponding carboxylic acids in refluxing dilute KOH in methanol before neutralising with HCl.

The ^{1}H NMR spectrum of the product shows seven unique environments (ESI†) for the protons on the bipyridyl fragment along with two sets of signals for the ethyl groups of the ester moieties. This is consistent with the cycloaddition of the acetylene to form the triazole and loss of magnetic equivalence of the two carboxylate groups. The resonances for the triazole-appended pyridine ring appear at δ 8.85, 8.67 and 7.61 and are shifted as a result of the cycloaddition relative to those of the azide starting material (δ 8.69, 8.15 and 7.34).[35]

Routes to ruthenium, iridium and rhenium dctzbpy complexes [Ru(bpy)$_2$(dctzbpy)][PF$_6$]$_2$ (**AS16**), [Ir(ppy)$_2$(dctzbpy)][PF$_6$] (**AS17**, ppyH = 2-phenylpyridine) and [Re(CO)$_3$(dctzbpy)Cl] (**AS18**) respectively were investigated involving direct reaction of the acid form of the ligand with precursor complexes, however, isolation of the corresponding complexes proved problematic. Isolation of complexes of the intermediate diester ligand, **AS16-Et$_2$**, **AS17-Et$_2$** and **AS18-Et$_2$**, followed by hydrolysis was deemed to give better results. Thus, two-step syntheses starting from [Ru(bpy)$_2$Cl$_2$], [Ir(ppy)$_2$Cl]$_2$ and [Re(CO)$_5$Cl] were carried out. Firstly, the above mentioned starting metal precursor complexes were reacted together with detzbpy (Scheme 1) followed by anion metathesis with NH_4PF_6 to yield the desired diester complexes.

As a consequence of the asymmetry of the detzbpy ligand the [Ru(bpy)$_2$] and [Ir(ppy)$_2$] fragments in **AS16-Et$_2$** and **AS17-Et$_2$** do not possess the C_2 symmetry present in **1** and **2**. Hence, each bpy and ppy ligand in **AS16-Et$_2$** and **AS17-Et$_2$** respectively is magnetically unique resulting in complicated ^{1}H NMR spectra due to the overlap of signals (ESI†). The ^{1}H NMR spectrum of **AS18-Et$_2$** exhibits detzbpy signals shifted to higher field in comparison with the free diester ligand by ~0.4 ppm with the resonances for the H-6 and H-6′ position appearing at δ 9.21 and 9.06 respectively.

The final dyes **AS16** to **AS18** can be readily accessed by hydrolysis with KOH in acetone and subsequent neutralisation. Due to solubility issues, however, and the fact that key properties are expected to differ little after hydrolysis electrochemical characterisation is reported for the more soluble esters **AS16-Et$_2$** to **AS18-Et$_2$**.

Cyclic voltammetry traces and summarised electrochemical data are presented in Fig. 4 and Table 1 respectively. The complex **AS16-Et$_2$** presents a reversible Ru(II)/(III) oxidation at +1.00 V and an irreversible reduction peak at −1.50 V assigned to the detzbpy reduction. This is followed by two further reversible reduction peaks assigned to the bpy ligands. A quasi-reversible oxidation is observed at +0.90 V for **AS17-Et$_2$**, corresponding to the one-electron Ir(III)/Ir(IV) couple. The first reduction presents as a quasi-reversible process at −1.59 V again assigned to be detzbpy ligand. Complex **AS18-Et$_2$** is

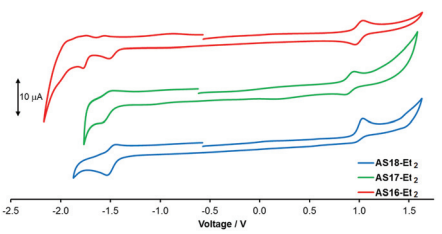

Fig. 4 Cyclic voltammetry traces for complexes **AS-16-Et$_2$**, **AS17-Et$_2$** and **AS18-Et$_2$** *vs.* Fc^+/Fc = 0.0 V.

Table 1 Summarised electrochemical data for complexes **AS16-Et$_2$** to **AS18-Et$_2$** at room temperature acetonitrile *vs.* Fc^+/Fc = 0.0 V

Dye	E_{ox}/V	E_{red}/V
AS16-Et$_2$	1.00	−1.50
AS17-Et$_2$	0.90	−1.59
AS18-Et$_2$	1.00	−1.56

characterised by a quasi-reversible oxidation peak at +1.00 V, in agreement with the potential of other $Re(CO)_3(dcb\text{-}Et_2)X$-based complexes (X = halide).[36] It also presents a reversible detzbpy-based reduction at −1.56 V. The oxidation potentials for these complexes are similar to those of their corresponding $dcbH_2$-based analogues consistent with the expectation of a largely metal-based HOMO.[29,36,37] The detzbpy-based reduction potentials (−1.5 to −1.6 V) are more cathodically shifted than that reported for **1** (−1.34 V)[29] consistent with a higher energy LUMO as indicated in the spectroscopic data.[17–19]

The isolated and purified complexes **AS16-Et$_2$** to **AS18-Et$_2$** were then refluxed in KOH/acetone and neutralised with HCl to yield the corresponding dctzbpy complexes. The analogous $dcbH_2$ complexes $[Ru(bpy)_2(dcbH_2)][PF_6]_2$ (**1**),[29] $[Ir(ppy)_2(dcbH_2)][PF_6]$ (**2**)[20] and $[Re(CO)_3(dcbH_2)(Cl)]$ (**3**)[17] were also prepared for comparison. UV-Visible absorption spectra were recorded for all complexes in acetonitrile solutions at room temperature and are presented in Fig. 5 with summarised data listed in Table 2.

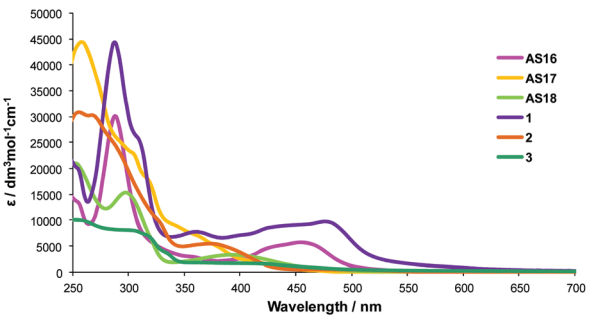

Fig. 5 UV-visible absorption spectra for complexes **AS16–18** and **1–3** in acetonitrile solutions.

Table 2 Summarised photophysical data for complexes **AS16–18** and their $dcbH_2$ analogues **1–3** at room temperature in acetonitrile

Complex	λ^{abs}/nm (ε/dm^3 mol^{-1} cm^{-1})	λ^{em}_{max}/nm	τ/ns
1	245 (21 923), 287 (44 481), 308 (26 079), 357 (7836), 430 (8807), 475 (9880)	682	32
2	256 (30 778), 289 (24 016), 377 (6905)	689	33
3	252 (10 289), 303 (8202), 413 (1826)	725	35
AS16	242 (15 624), 287 (30 138), 424 (4642), 456 (5719)	638	34
AS17	255 (44 311), 301 (23 330), 364 (7771), 415 (1914)	590	25
AS18	254 (20 204), 297 (15 317), 397 (3815)	553	38

The comparison between the $dcbH_2$ complexes and their dctzbpy analogues shows similar absorption profiles but with a slight blue shift in the lower energy absorptions for complexes **AS16–18**. All complexes show a strong band at 250–300 nm attributed to π–π* ^{1}LC transitions together with ^{1}MLCT bands of modest intensity ($\varepsilon \approx 5000$–$10\,000$ dm^3 mol^{-1} cm^{-1}) above 400 nm. The blue-shifted absorption bands in the spectra of the dctzbpy complexes suggests that the LUMO is higher in energy than those for the $dcbH_2$ analogues and that the biscarboxytriazole group is less electron withdrawing than the two carboxylate groups bonded directly to the bipyridyl core in $dcbH_2$. Nevertheless, LUMO is correctly positioned with reference to the TiO_2 Fermi level for favourable charge injection when adsorbed on a photoanode.[4] These similar absorption patterns will be expected to result in comparable photovoltaic performance for the dyes **AS16–18** relative to **1–3**.

The complexes **AS16–18** exhibit broad emission bands between 550 and 650 nm which are similarly blue-shifted relative to their $dcbH_2$ analogues, with similar life-times at about 32 ns. This again is indicative that the LUMO of the dctzbpy ligand, and thus that of its complexes, is higher in energy with respect to $dcbH_2$ thereby leading to the observed destabilisation of ^{3}MLCT T_1 states in these complexes.

In order to gain a more complete understanding of the photophysical and electrochemical properties imparted by the new ligand dctzbpy we turned to density functional theory (DFT) calculations. These calculations were carried out on the free acid carboxylic acid complexes **AS16–18**, partly to reduce computational cost of the extra alkyl groups of the ester moieties, and due to the fact that the spectroscopic absorption properties of the free acid and ester complexes differ little suggesting that they are electronically very similar. Optimised singlet ground state geometries for the three new dyes **AS16–18** and model complexes **1–3** were calculated at the B3LYP level of theory using Stuttgart–Dresden relativistic small-core effective core potentials and basis sets for the metallic elements and 6-311G* basis sets for all other atoms. Molecular orbital energies (Fig. 6) and localisations (Fig. 7) were then determined in single-point calculations using the COSMO solvation model (ε = 37.5 for acetonitrile). The HOMO has significant metallic d-orbital character in all cases with additional aryl π* character in the case of **AS17** and CO π* and Cl p-orbital character for **AS18**. In all cases the LUMO is dominated by the dctzbpy ligand and is mostly localised over the bpy fragment. For **AS16** there is also a minor contribution

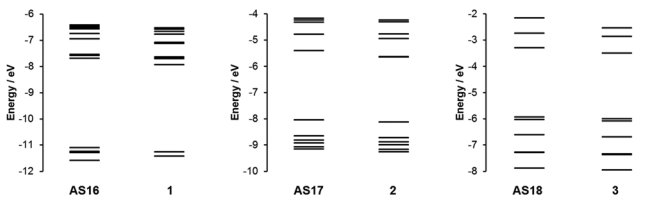

Fig. 6 Calculated molecular orbital energy level diagram for complexes **AS16–18** and **1–3**.

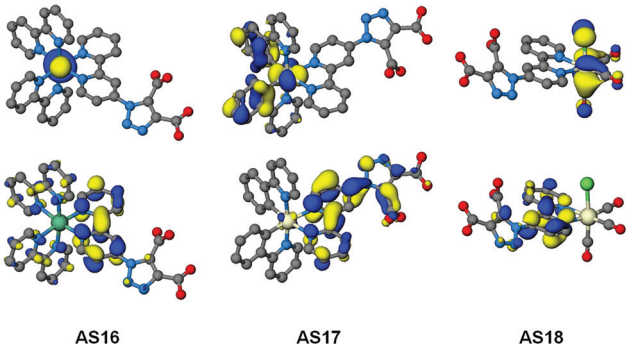

Fig. 7 Optimised geometries and plots of HOMO (top) and LUMO (bottom) orbitals for complexes **AS16** to **AS18**.

from the bpy ligands whilst for **AS17** and **AS18** there is an additional contribution from the dicarboxytriazole moiety.

Frontier molecular orbital energies are provided in Table 3. In agreement with UV-visible absorption and emission data there is a slight destabilization of both HOMO and LUMO orbitals, but to a greater extent for the latter, for **AS16–18** relative to those of their $dcbH_2$ analogues. Thus the HOMO–LUMO gaps for the dctzbpy complexes are an average of 0.12 eV larger than for **1–3** accounting for the experimental spectroscopic data. The ground state frontier molecular orbitals of **AS16–18** are thus correctly localised to facilitate optimum charge-transfer directionality with respect to the carboxylate anchor for efficient charge injection when adsorbed onto a photoanode. Moreover, the relative energy of the dctzbpy ligand localised LUMO in complexes **AS16–18**, being slightly higher than those of the $dcbH_2$ analogues **1** to **3**, will inevitably be favourably positioned relative the TiO_2 Fermi level in order to facilitate charge injection into the electrode.

Time-dependent DFT (TDDFT) calculations were carried out on the optimised ground state geometries of each complex in order to determine vertical excitation energies and the nature of the lowest energy singlet excited states. Simulated absorption spectra are overlaid with experimental spectra and shown in Fig. 8 and reveal that predicted transitions correlate well with the experimental spectra. The excitations to the S_1 state of all complexes are primarily HOMO → LUMO in character, however, they are of low oscillator strength and will therefore contribute little to the observed absorption spectra. Consistent with the enlarged HOMO–LUMO gap in complexes **AS16–18** relative to their respective $dcbH_2$ analogues the S_1 transitions

Table 3 Calculated HOMO and LUMO energies for complexes **AS16–18** and **1–3**

Dye	LUMO/eV	HOMO/eV	HOMO–LUMO/eV
1	−7.92	−11.26	3.33
AS16	−7.68	−11.10	3.42
2	−5.65	−8.13	2.48
AS17	−5.41	−8.04	2.63
3	−3.51	−6.00	2.49
AS18	−3.30	−5.94	2.64

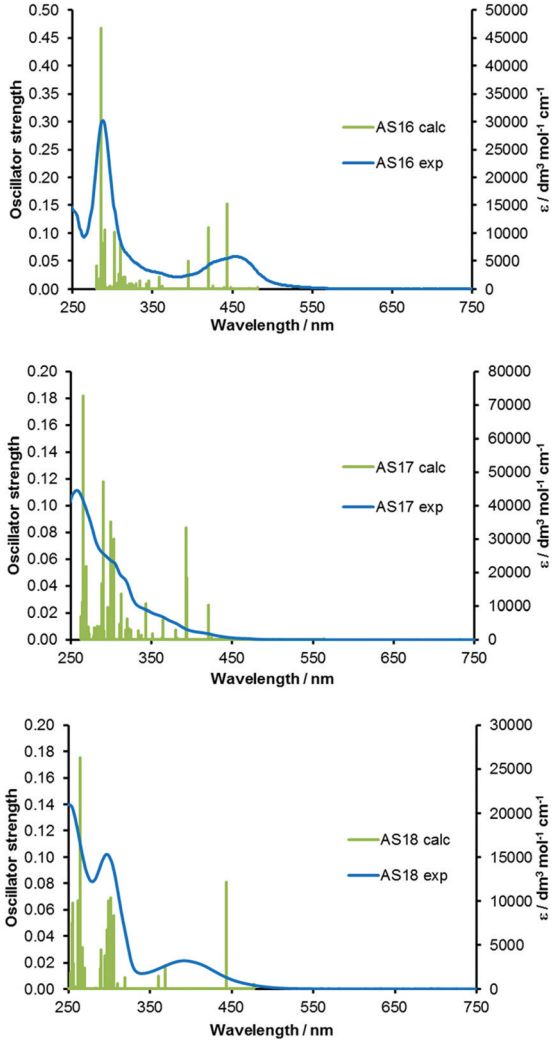

Fig. 8 TDDFT calculated absorption spectra for complexes **AS16–18** with experimental spectra overlaid.

occur at shorter wavelengths. The major transitions observed for all complexes between 350 and 550 nm are primarily of ^{1}MLCT character. Higher energy intense absorptions (240 to 350 nm) are assigned as having predominantly ^{1}LC π → π* character. The ruthenium complex **AS16** presents two dominating transitions at 452 (S_5) and 412 (S_8) nm respectively, involving primarily HOMO−2 → LUMO+2 ^{1}MLCT character. The iridium complex **AS17** exhibits one transition at 421 nm (S_4) of mainly HOMO−1 → LUMO ^{1}MLCT/^{1}LLCT character and two transitions at 394 (S_5) and 393 (S_6) nm with ^{1}MLCT/^{1}ILCT and ^{1}MLCT/^{1}LLCT character respectively. The rhenium complex **AS18** exhibits a strong transition at 443 nm (S_2) with a predominant composition of HOMO−1 → LUMO ^{1}MLCT character.

The relative positioning of the frontier orbitals in the dctzbpy complexes described would indeed seem to make them amenable to application in the photovoltaic sensitisation of n-type solar cells. We therefore prepared n-type TiO_2-based test DSSC devices utilising complexes **AS16** to **AS18** along with those of the corresponding $dcbH_2$ analogues for comparison.

The free dye **AS16** and TiO_2-immobilised **AS16** were analysed by FTIR spectroscopy and microscopy in an attempt to gain insight into the anchoring mode of the dctzbpy ligand. Unfortunately the data do not enable any definitive conclusions to be drawn.

The principle photovoltaic parameters for the constructed DSSC devices are listed in Table 4. The overall conversion efficiencies η were derived from the equation $\eta = J_{sc}V_{oc}FF$, where J_{sc} is the short circuit current density, V_{oc} is the open circuit voltage, and FF is the fill factor. Fig. 9 shows the photocurrent–voltage and IPCE traces of the n-type DSSCs based on the new dyes.

The IPCE values are generally below 10% over the visible region of the spectrum except for those of **AS16** and **2** (Fig. 9). The IPCE profiles reflect the absorption profiles of the corresponding dyes; both **AS16** and **1** exhibit IPCE maxima coincident with the region in which the complexes have a ^{1}MLCT-based absorption band between 400–500 nm. All the other complexes have absorption maxima between 370 and 420 nm so their IPCE curves show only the tail of these bands into the visible region.

The obtained photovoltaic efficiencies for complexes **AS17** and **AS18** are lower than those for their $dcbH_2$ analogues determined under identical conditions. This is not unexpected and attributable to their blue-shifted absorption profiles which would result in lower light harvesting efficiency. Further, whilst the LUMO energies for **AS16–18** are expected to be in the correct position relative to the TiO_2 Fermi level they are higher in energy than those of **1–3**. This might imply less efficient overlap of the LUMO with the TiO_2 conduction band and consequently lower electron injection efficiency. The best result for the new dyes is obtained for complex **AS16** with an efficiency of 0.61% (compared to 0.1% for **1** and 5.76% for the benchmark dye **N719** under the same conditions). **AS16** achieved the highest open circuit voltage (0.66 V) which might suggest a longer excited state electron lifetime,[38] hence a higher electron density on the TiO_2 surface. The efficiency for **AS17** was dramatically lower than that of its $dcbH_2$ analogue **2**. Indeed, the efficiency of **2** (0.71%) exceeds that of **AS16** with a reasonably strong optical absorption shoulder when adsorbed on TiO_2 (ESI†) that matches the band at 450–550 nm apparent in the IPCE trace. The rhenium complexes **AS18** and **3**, however, showed very similar J_{sc}, V_{oc} and η values to each other.

Table 4 Photovoltaic parameters of tested dyes **AS16–18** and **1–3** with **N719** as a benchmark comparison in TiO_2-based n-type DSSC devices. The electrolyte contained 0.6 M tetrabutylammonium iodide, 0.015 M I_2, 0.1 M guanidinium thiocyanate and 0.5 M 4-*tert*-butylpyridine in MeCN

Dye	J_{sc}/mA cm^{-2}	V_{oc}/mV	FF/%	η/%	IPCE/%
N719	10.7	779	69	5.76	65
1	0.39	457	57	0.1	6
AS16	1.18	662	78	0.61	15
2	1.44	633	78	0.71	17
AS17	0.06	485	72	0.02	3
3	0.36	495	73	0.13	6
AS18	0.24	532	73	0.09	5

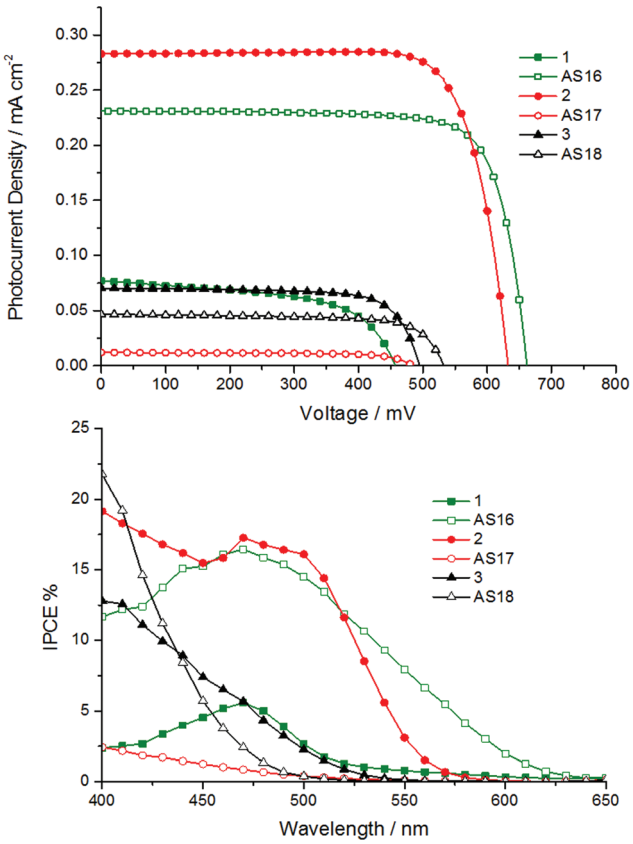

Fig. 9 Current–voltage traces for pilot TiO_2-based n-type DSSC devices utilising complexes **AS16** to **AS18** and model dyes **1** to **3** (top) along with IPCE traces for each cell (bottom). The electrolyte contained 0.6 M tetrabutylammonium iodide, 0.015 M I_2, 0.1 M guanidinium thiocyanate and 0.5 M 4-*tert*-butylpyridine in MeCN.

Whilst **AS16** indeed shows superior performance over its $dcbH_2$ model in the cells test the performance of the other new dyes, especially in the case of **AS17**, is disappointing and likely stems from the elevated LUMO associated with the dctzbpy ligand. However, we reasoned that these dyes may yield greater sensitisation efficiency than their $dcbH_2$ analogues in p-type devices for the very same reason.[24] We therefore constructed and tested NiO-based p-type cells based on the new dyes and their $dcbH_2$ analogues **1** to **3** along with coumarin C343 as a benchmark comparison. Current–voltage and IPCE plots are provided in Fig. 10 with photovoltaic parameters listed in Table 5.

The **AS16** based cell exhibits the highest overall efficiency of all metal complex sensitised p-type cells (0.028% compared to 0.01% for C343) and the highest IPCE of 17%. As might be expected due to the dctzbpy anchoring ligand being less electron withdrawing than $dcbH_2$ the performances of cells using **AS16** and **AS17** exceed those of **1** and **2** respectively. Indeed, **1** and **2** seem to be desensitisers of NiO in these cells with the current generated below 450 nm most likely stemming from photolysis of the I_3^- electrolyte as previously noted by Nattestad *et al.*[39] Cells utilising **AS18** and **3** yield near identical performance parameters.

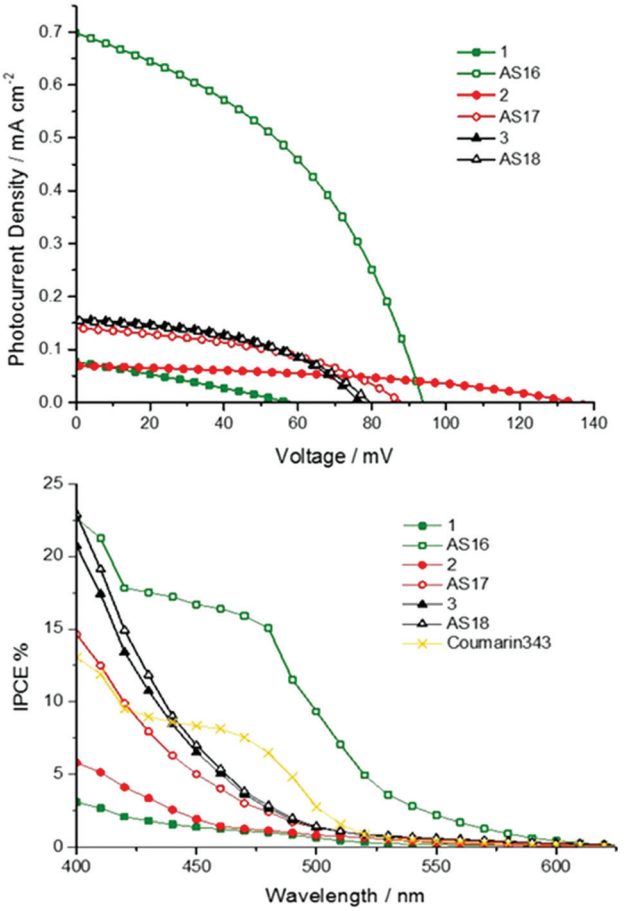

Fig. 10 Current–voltage traces for pilot NiO-based p-type DSSC devices utilising complexes **AS16** to **AS18** and model dyes **1** to **3** (top) along with IPCE traces for each cell (bottom). The electrolyte contained 0.1 M I_2 and 1 M LiI in MeCN.

Table 5 Photovoltaic parameters of tested dyes **AS16–18** and **1–3** with Coumarin-C343 as a benchmark comparison in NiO-based p-type DSSC devices. The electrolyte contained 0.1 M I_2 and 1 M LiI in MeCN

Dye	J_{sc}/mA cm^{-2}	V_{oc}/mV	FF/%	η/%	IPCE/%
C343	0.26	105	37	0.01	8
1	0.076	58	27	0.0012	2
AS16	0.69	94	42	0.028	17
2	0.069	134	40	0.0037	3
AS17	0.14	89	42	0.0052	5
3	0.16	77	45	0.0056	6
AS18	0.15	79	46	0.0055	6

The results for **AS16** are generally encouraging in terms of dye development but are disappointing when considered in comparison to the benchmark **N719**. With further ancillary ligand development in combination with the new ligand it may be possible to arrive at much higher efficiency n-type sensitisers. Complexes of the new anchoring ligand dctzbpy may also find potential applications in p-type cells since the data show that the ruthenium(II)-based dye **AS16** results in an efficiency three times that of the benchmark standard dye coumarin-C343. When combined with other ligands about a metal centre with greater electron withdrawing character this anchoring ligand provides potential for the development of far more efficient p-type sensitisers. Complexes based on the ligands described here may also find utility as photochemical solar fuel catalysts adsorbed on semiconductor nanoparticles.[40] As the complexes here are luminescent and the carboxylate groups can be utilised for bioconjugation complexes bearing the dctzbpy core structure could also be used in biological imaging applications.[41]

Conclusions

We have designed and prepared a new anchoring ligand, 1-(2,2′-bipyridin-4-yl)-1,2,3-triazole-4,5-dicarboxylic acid, and its ruthenium, iridium and rhenium complexes. New ruthenium(II), iridium(III) and rhenium(I)-based dyes, **AS16** to **AS18** respectively, have been compared with their $dcbH_2$ analogues. Spectroscopic and theoretical results suggest the LUMO of the dctzbpy ligand is higher in energy than that of $dcbH_2$. Whilst correctly positioned for charge injection upon photoexcitation the resultant blue shift in optical absorption bands results in inferior light harvesting properties. Whilst improved photovoltaic performance is observed for **AS16** this leads to a reduction in the photovoltaic efficiency for the other dyes in n-type DSSCs when compared to their $dcbH_2$ analogues. In p-type cells the ruthenium(II) and iridium(III)-based dyes **AS16** and **AS17** display superior performance over their $dcbH_2$ counterparts. Indeed, **AS16** is shown to yield three times the efficiency of the benchmark dye coumarin C343. The work therefore offers insights into new anchor ligand systems. The newly reported ligand has potential for further development for dye complexes in NiO-based p-type DSSC devices especially in which a less electron withdrawing anchoring ligand is desirable, and in other applications including dye-sensitised electrochemical cells for solar catalysis and biological luminescent imaging.

Experimental section

General methods

Chemicals were purchased from Aldrich and Acros, iridium and ruthenium were purchased from Precious Metal Online (Australia) and used as received. All complexation reactions were carried out under nitrogen. 4-Azido-2,2′-bipyridine,[34] $[Ru(bpy)_2Cl_2]$,[24] $[Ir(ppy)_2Cl]_2$,[20] $[Ru(bpy)_2(dcbH_2)][PF_6]_2$ (**1**),[18] $[Ir(ppy)_2(dcbH_2)][PF_6]$ (**2**),[20] $[Re(CO)_3(Cl)(dcbH_2)]$ (**3**),[17] were all prepared according to literature procedures. ^{1}H NMR and ^{13}C NMR spectra were recorded on a Bruker Avance 400 MHz instrument. Mass spectrometry data were collected on a Bruker Micro Q-TOF instrument. UV-Visible absorption spectra were recorded on a Varian Cary 300 spectrophotometer and corrected emission spectra were recorded on a Horiba Fluoromax-4 spectrofluorometer. Luminescent lifetime measurements were carried out using an Edinburgh Instruments Mini-Tau spectrometer.

Electrochemistry

For the cyclic voltammetry a EmStat3 electrochemical interface (Palm Sens, Netherlands) was employed, voltammograms were plotted on PSTrace software (Palm Sens, Netherlands). Cyclic voltammetry was carried out in a single compartment three electrode electrochemical cell under nitrogen atmosphere. Glassy carbon, platinum and Ag/AgCl were used respectively as working, counter and reference electrodes. The potential of the tested electrode was measured *versus* ferrocinium/ferrocene standard internal reference ($FeCp_2^+/FeCp_2$). The electrolyte used for the cyclic voltammetry measurements was 0.1 M $TBAPF_6$ in acetonitrile, prior to measurements all the solutions were degassed with nitrogen and during measurements a nitrogen blanket was maintained over the solution. The data were then plotted as current *vs.* voltage.

Dye sensitised solar cell fabrication

FTO glass was used as current collector (TCO30-10, 3 mm thick glass substrate with a 10 Ω sq^{-1}). For TiO_2-based anodes cleaned and dried FTO electrodes were immersed into a 40 mM aqueous $TiCl_4$ solution at 70 °C for 30 minutes and washed with pure water and ethanol and dried. A layer of nanocrystalline TiO_2 paste (Solaronix Ti-Nanoxide SP-T) was coated on the FTO glass plates by doctor blade technique, using a round mask (5 mm diameter, 0.25 cm^2 area) made by adhesive tape (3M Magic). The film was dried for 5 minutes on a hotplate and a second layer of TiO_2 was deposited as before. Following this a light scattering layer (Solaronix Ti-Nanoxide R/SP) was applied in the same way and the films were sintered at 500 °C for 30 minutes. After a second treatment with $TiCl_4$, the films were sintered for a final time as before. After cooling to 80 °C, the TiO_2 electrodes were immersed into a 0.5 mM dye solution in acetonitrile overnight in the dark.

The NiO films were prepared by using an F108-templated precursor solution containing $NiCl_2$ (1 g), Pluronic® copolymer F108 (1 g), distilled water (3 g) and ethanol (6 g) and the excess was removed by doctor blade. The film was sintered at 450 °C for 30 minutes and additional layers of precursor solution were applied and sintered until the film thickness was *ca.* 1.5 μm.

The Pt catalyst was deposited on the FTO glass, coating with 10 μL cm^{-2} of H_2PtCl_6 solution (5 mM ethanol solution), air dried and heated at 400 °C for 15 minutes. The dye-covered TiO_2 or NiO electrodes and Pt-counter electrodes were assembled into a sandwich-type cell and sealed with a Surlyn hot-melt gasket of 60 μm thickness. A solution of 0.5 M TBP, 0.015 M I_2, 0.6 M TBAI and 0.1 M GuSCN in acetonitrile was used as electrolyte in the TiO_2-based n-type cells whereas an electrolyte containing 0.1 M I_2 and 1 M LiI in acetonitrile was used for p-type cells.

Computational methods

DFT calculations were carried out using the NWChem 6.3 software package.[42] B3LYP hybrid functional (20% Hartree–Fock) method has been used for calculations,[43,44] Stuttgart relativistic small core ECP[45] for transition metals and 6-311G* [46] basis sets for all other atoms. Molecular geometries and molecular orbitals pictures were realised using the ccp1 graphical software. For all the studied complexes, the ground state geometries were first optimized and molecular orbital energies determined. TDDFT calculations[47] on optimised structures in CH_3CN by using the COSMO solvation model,[48] built in NWChem software, were used to obtain the electronic spectra and molecular orbital energy levels.

Synthesis of diethyl-1-(2,2′-bipyrid-4-yl)-1,2,3-triazole-4,5-dicarboxylate

4-Azido-2,2′-bipyridine (0.1 g, 0.51 mmol) and diethyl acetylenedicarboxylate (0.16 g, 0.76 mmol) was dissolved in toluene (15 mL). The solution was allowed to stir at 70 °C for 24 h. The solvent was removed under vacuum and the product was recrystallised from DCM and hexane to yield a white solid. (175 mg, yield 93%).

^{1}H NMR (400 MHz, $CDCl_3$) δ: 8.85 (d, ^3J = 5.28 Hz, 1H, py-*H*); 8.67 (d, ^3J = 2.08 Hz, 1H, py-*H*); 8.65 (d, ^3J = 4.44 Hz, 1H, py-*H*); 8.45 (d, ^3J = 7.92 Hz, 1H, py-*H*); 7.83 (td, ^3J = 7.72, ^4J = 1.72 Hz, 1H, py-*H*); 7.61 (dd, ^3J = 5.28, ^4J = 2.16 Hz, 1H, py-*H*); 7.43 (ddd, 1H, ^3J = 7.52, ^4J = 4.77, ^5J = 1.00, py-*H*); 4.47 (q, ^3J = 7.12, 2H, C*H*$_2$–CH$_3$); 4.46 (q, ^3J = 7.12, 2H, C*H*$_2$–CH$_3$); 1.41 (t, ^3J = 7.12 Hz, 3H, CH$_2$–C*H*$_3$); 1.35 (t, ^3J = 7.16 Hz, 3H, CH$_2$–C*H*$_3$).

^{13}C{^{1}H} NMR (100 MHz, $CDCl_3$) δ: 159.45, 158.90, 158.61, 154.21, 150.91, 149.38, 143.36, 139.38, 137.12, 132.45, 124.69, 121.24, 117.37, 114.59, 63.93, 62.09, 14.20, 13.77.

HRMS (ESI) *m*/*z* calcd for $C_{18}H_{17}N_5O_4$ 367.1280, found 368.1359 $(M + H)^+$.

Synthesis of 1-[2,2′-bipyridine-4-yl]triazole-4,5-dicarboxylic acid

1-[2,2′-Bipyridine-4-yl]triazole-4,5-ethyldicarboxylate (0.1 g, 0.51 mmol) was dissolved in 25 mL of NaOH 0.1 M and heated to reflux temperature for 4 h, after that the solution was neutralised with HCl 2 M. A white solid crushed out, collected by filtration and dried under reduced pressure. (134.84 mg, yield 85%).

^{1}H NMR (400 MHz, DMSO-d_6) δ: 8.96 (d, ^3J = 5.24, 1H, py-*H*); 8.77 (d, ^3J = 4.72, 1H, py-*H*); 8.61 (d, ^4J = 1.36, 1H, py-*H*); 8.54 (d, ^3J = 7.96, 1H, py-*H*); 8.15 (t, ^3J = 7.64, 1H, py-*H*); 7.81 (d, ^3J = 5.20, ^4J = 1.72, 1H, py-*H*); 7.64 (t, ^3J = 5.48, 1H, py-*H*).

^{13}C{^{1}H} NMR (100 MHz, DMSO-d_6) δ: 160.67, 158.62, 155.34, 152.77, 150.66, 148.55, 144.94, 139.97, 139.14, 134.14, 125.4, 121.45, 120.7, 116.84.

HRMS (ESI) *m*/*z* calcd for $C_{14}H_9N_5O_4$ 311.0654, found 310.0582 $(M - H)^-$.

Synthesis of [Ru(bpy)$_2$(diethyl-1-(2,2′-bipyrid-4-yl)-1,2,3-triazole-4,5-dicarboxylate)](PF$_6$)$_2$ AS16-Et$_2$

100 mg of $Ru(bpy)_2Cl_2$ were dissolved in EtOH (20 mL) together with 113 mg of dectzbpy. The solution was heated to reflux temperature overnight, under N_2 in the dark. The solvent was removed under reduced pressure and the resulting solid dissolved in MeOH, an excess of NH_4PF_6 was added and an orange crystalline solid was collected by filtration. The solid

was columned on silica gel with MeCN : H_2O : KNO_3 7 : 1 : 0.5 as eluent. The main gloving fraction was then dried, redissolved in acetonitrile and filtered. The filtrate was dried and redissolved in a minimum amount of methanol, NH_4PF_6 was added, an orange solid crashed and it was collected by filtration. (168.1 mg, yield 76%).

^{1}H NMR (400 MHz, CD_3CN) δ: 8.79 (d, ^3J = 2.02, 1H, bpy-*H*); 8.55–8.49 (m, 5H, bpy-*H*); 8.12–8.05 (m, 5H, bpy-*H*); 7.96 (d, ^3J = 6.15, 1H, bpy-*H*); 7.83 (d, ^3J = 5.32, 1H, bpy-*H*); 7.78 (d, ^3J = 5.53, 1H, bpy-*H*); 7.76–7.69 (m, 3H, bpy-*H*); 7.55 (dd, ^3J = 6.15, ^3J = 2.20, 1H, bpy-*H*); 7.48–7.39 (m, 5H, bpy-*H*); 4.43 (q, ^3J = 7.16, 2H, C*H*$_2$–CH_3); 4.31 (q, ^3J = 7.07, 2H, C*H*$_2$–CH_3) 1.37 (t, ^3J = 7.12, 3H, CH_2–C*H*$_3$); 1.11 (t, ^3J = 7.03, 3H, CH_2–C*H*$_3$).

^{13}C{^{1}H} NMR (100 MHz, CD_3CN) δ: 159.54; 159.10; 157.74; 156.97, 156.96; 156.93, 156.92; 156.88, 156.87; 156.83; 156.05; 153.52; 152.00; 151.94; 151.91; 151.83; 151.65; 143.10; 140.54, 138.19; 138.10; 138.09; 137.94, 128.41; 127.78; 127.74; 127.70; 127.62; 125.12; 125.08, 124.48; 124.43; 122.04; 119.67; 63.75; 62.25; 13.40; 13.04.

HRMS (ESI) *m*/*z* calcd for $[C_{38}H_{33}N_9O_4Ru]^{2+}$ 390.5860, found 390.5864 $(M)^{2+}$.

Synthesis of [Ru(bpy)$_2$(1-[2,2′-bipyridine-4-yl]triazole-4,5-ethyldicarboxylic acid)]PF_6 AS16

50 mg of $[Ru(bpy)_2(detzbpy)](PF_6)_2$ was dissolved in 8 mL 1 M KOH/acetone 1 : 1 and heated to reflux temperature for 12 hours. After cooling the acetone was removed under vacuum and the solution was neutralised with 1 M HCl. The solution was concentrated and a solid crashed out. The solid was collected by filtration, redissolved in a minimal amount of methanol and NH_4PF_6 was added, newly a red solid crashed and it was collected by filtration. (35.5 mg, yield 75%).

^{1}H NMR (400 MHz, CD_3CN) δ: 8.76 (d, ^3J = 2.08, 1H, bpy-*H*); 8.55–8.46 (m, 5H, bpy-*H*); 8.13–8.03 (m, 5H, bpy-*H*); 7.92 (d, ^3J = 6.12, 1H, bpy-*H*); 7.83–7.70 (m, 5H, bpy-*H*); 7.61 (d, ^3J = 6.12, ^4J = 2.2, 1H, bpy-*H*); 7.51–7.40 (m, 5H, bpy-*H*).

^{13}C{^{1}H} NMR (100 MHz, CD_3CN) δ: 159.68, 159.63, 159.21, 157.86, 157.03, 156.99, 156.94, 156.90, 156.88, 156.46, 156.23, 154.69, 152.38, 151.89, 151.86, 151.84, 151.82, 151.81, 151.62, 143.42, 138.08, 138.03, 138.00, 137.96, 128.03, 127.73, 127.72, 127.66, 127.65, 124.75, 124.43, 124.40, 124.31, 121.72, 120.59.

Synthesis of [Ir(ppy)$_2$(diethyl-1-(2,2′-bipyrid-4-yl)-1,2,3-triazole-4,5-dicarboxylate)]PF_6 AS17-Et$_2$

107 mg of $[Ir(ppy)_2Cl]_2$ dimer were dissolved in DCM : MeOH 2 : 1 (12 mL) together with 77 mg of detzbpy and 53 mg of $AgPF_6$. The solution was heated to reflux temperature overnight, under N_2 in the dark. The solvent was removed under reduced pressure and the resulting solid dissolved in DCM and filtered on celite pad. The solvent was removed again and the solid recrystallised from acetonitrile/ether. A pale orange solid was collected by filtration and columned with 10% MeOH in DCM. (149.3 mg, yield 74%).

^{1}H NMR (400 MHz, CD_3CN) δ: 8.81 (d, ^3J = 1.70, 1H, bpy-*H*); 8.54 (d, ^3J = 8.04, 1H, bpy-*H*); 8.20–8.13 (m, 2H, bpy-*H*); 8.08 (d, ^3J = 8.14, 2H, ppy-*H*); 8.02 (dd, ^3J = 5.78, ^4J = 0.78, 1H, bpy-*H*); 7.86 (td, ^3J = 7.35, ^4J = 0.84, 2H, ppy-*H*); 7.82 (d, ^3J = 7.62, 2H, ppy-*H*); 7.72 (dd, ^3J = 5.52, ^3J = 0.81, 1H, ppy-*H*); 7.65 (dd, ^3J = 6.09, ^4J = 2.17, 1H, bpy-*H*); 7.63 (dd, ^3J = 5.96, ^4J = 0.81, 1H, bpy-*H*); 7.56 (t, ^3J = 6.30, 1H, bpy-*H*); 7.09–7.02 (m, 4H, ppy-*H*); 6.96–6.90 (m, 2H, ppy-*H*); 6.29 (dd, ^3J = 7.75, ^4J = 0.88, 1H, ppy-*H*); 6.26 (dd, ^3J = 7.63, ^4J = 0.74, 1H, ppy-*H*); 4.42 (q, ^3J = 6.95, 2H, C*H*$_2$–CH_3); 4.31 (qd, ^3J = 7.10, ^4J = 1.15, 2H, C*H*$_2$–CH_3); 1.36 (t, ^3J = 7.10, 3H, CH_2–C*H*$_3$); 1.10 (t, ^3J = 7.10, 3H, CH_2–C*H*$_3$).

^{13}C{^{1}H} NMR (100 MHz, CD_3CN) δ: 167.35, 167.24, 159.48, 158.15, 157.72, 154.72, 152.48, 150.99, 149.52, 149.49, 149.43, 144.40, 144.09, 143.97, 140.50, 139.62, 138.78, 138.72, 131.80, 131.59, 131.44, 130.49, 130.44, 129.26, 125.37, 124.98, 124.95, 123.66, 123.54, 123.08, 122.82, 122.76, 120.10, 120.01, 119.98, 63.81, 62.24, 13.39, 12.97.

HRMS (ESI) *m*/*z* calcd for $[C_{40}H_{33}N_7O_4Ir]^+$ 867.2230, found 867.2228 (M^+).

Synthesis of [Ir(ppy)$_2$(1-[2,2′-bipyridine-4-yl]triazole-4,5-ethyldicarboxylate)]PF_6 AS17

50 mg of **AS17-Et$_2$** was dissolved in 8 mL 1 M KOH/acetone 1 : 1 and heated to reflux temperature for 12 hours. After cooling the acetone was removed under vacuum and the solution was neutralised with 1 M HCl. The solution was concentrated and a solid crashed out. The solid was collected by filtration, redissolved in a minimal amount of methanol and NH_4PF_6 was added, newly a yellow solid crashed and it was collected by filtration. (32.1 mg, yield 68%).

^{1}H NMR (400 MHz, CD_3CN) δ: 8.46 (d, ^3J = 6.56 Hz, 1H, bpy-*H*); 8.11 (td, ^3J = 6.28, ^4J = 1.24 Hz, 1H, bpy-*H*); 8.07 (t, ^3J = 5.64 Hz, 2H, ppy-*H*); 8.00 (bs, 1H, bpy-*H*); 7.97 (dd, ^3J = 4.3, ^4J = 0.8 Hz, 1H, bpy-*H*); 7.89–7.84 (m, 2H, ppy-*H*); 7.81 (d, ^3J = 6.08 Hz, 2H, ppy-*H*); 7.71 (d, ^3J = 4.72 Hz, 1H, bpy-*H*); 7.65 (d, ^3J = 4.6 Hz, 1H, ppy-*H*); 7.63 (d, ^3J = 5.16 Hz, 1H, ppy-*H*); 7.47 (td, ^3J = 5.24, ^4J = 0.72 Hz, 1H, bpy-*H*); 7.09–7.02 (m, 5H, bpy-*H*&ppy-*H*); 6.97–6.9 (m, 3H, ppy-*H*); 6.31 (dd, ^3J = 6.06, ^4J = 0.6 Hz, 1H, ppy-*H*); 6.28 (dd, ^3J = 6.04, ^4J = 0.52 Hz, 1H, ppy-*H*).

^{13}C{^{1}H} NMR (100 MHz, CD_3CN) δ: 167.63, 167.49, 157.16, 156.23, 151.26, 150.45, 149.14, 149.11, 144.28, 144.06, 139.99, 139.88, 139.86, 139.84, 139.21, 139.16, 138.36, 138.33, 131.91, 131.67, 131.65, 131.51, 130.31, 130.27, 130.23, 128.11, 124.82, 124.78, 124.33, 123.4, 123.37, 122.32, 122.3.

Synthesis of Re(CO)$_3$(diethyl-1-(2,2′-bipyrid-4-yl)-1,2,3-triazole-4,5-dicarboxylate)Cl AS18-Et$_2$

100 mg of $[Re(CO)_5Cl]$ and 113 mg of detzbpy were dissolved in 25 mL of toluene and heated at 70 °C for 12 hours. After cooling the volume was reduced under reduced pressure and a yellow solid crashed out, it was collected by filtration and dried with diethylether. (155.8 mg, yield 84%).

^{1}H NMR (400 MHz, CD_3CN) δ: 9.21 (d, ^3J = 5.96, 1H, bpy-*H*); 9.06 (dd, ^3J = 5.38, ^3J = 0.70, 1H, bpy-*H*); 8.70 (d, ^3J = 2.10, 1H, bpy-*H*); 8.44 (d, ^3J = 8.18, 1H, bpy-*H*); 8.23 (dt, ^3J = 7.95 1.52, 1H, bpy-*H*); 7.78 (dd, ^3J = 6.08, ^3J = 2.34, 1H, bpy-*H*); 7.69 (dt, ^3J = 6.49, ^3J = 1.22, 1H, bpy-*H*); 4.44 (q, ^3J = 7.13, 2H, C*H*$_2$–CH_3);

4.41 (q, ^3J = 7.02, 2H, CH_2–CH_3); 1.38 (t, ^3J = 7.13, 3H, CH_2–CH_3); 1.27 (t, ^3J = 6.98, 3H, CH_2–CH_3).

$^{13}C\{^1H\}$ NMR (100 MHz, CD3CN) δ: 197.63, 197.47, 189.26, 159.55, 157.96, 157.87, 154.73, 154.65, 153.25, 144.91, 140.59, 140.22, 131.79, 128.29, 124.65, 121.86, 119.36, 63.94, 62.24, 13.40, 13.07.

HRMS (ESI) m/z calcd for $C_{21}H_{17}ClN_5O_7Re$ 671.0352, found 689.0694 $(M + NH_4)^+$.

Synthesis of Re(CO)$_3$(1-[2,2′-bipyridine-4-yl]triazole-4,5-ethyldicarboxylate)Cl AS18

50 mg of [Re(CO)$_3$(detzbpy)Cl] was dissolved in 8 mL 1 M KOH/acetone 1 : 1 and heated to reflux temperature for 12 hours. After cooling the acetone was removed under vacuum and the solution was neutralised with 1 M NaOH. The solution was concentrated and a yellow solid crashed out. The solid was collected by filtration. (30.7 mg, yield 67%).

^1H NMR (400 MHz, DMSO-d$_6$) δ: 8.94 (d, ^3J = 5.44, 1H, bpy-*H*); 8.44 (d, ^3J = 8.17, 1H, bpy-*H*); 8.22 (t, ^3J = 7.78, 1H, bpy-*H*); 7.97 (d, ^3J = 6.81, 1H, bpy-*H*); 7.63 (t, ^3J = 6.61, 1H, bpy-*H*); 7.15 (d, ^3J = 2.25, 1H, bpy-*H*); 6.14 (dd, ^3J = 6.95, ^4J = 2.64, 1H, bpy-*H*).

$^{13}C\{^1H\}$ Low solubility, NMR not recorded.

Acknowledgements

The authors wish to thank the Leverhulme Trust and the University of Huddersfield for funding this research. As a member of the UK Materials Chemistry Consortium PIPE also thank the EPRSC (EP/L000202) and the UK HPC national resource, Archer, as well as the University of Huddersfield High Performance Computing Research Group for computational resources utilised in this project.

References

1 A. Hagfeldt, G. Boschloo, L. Sun, L. Kloo and H. Pettersson, *Chem. Rev.*, 2010, **110**, 6595–6663.
2 M. K. Nazeeruddin, E. Baranoff and M. Grätzel, *Sol. Energy*, 2011, **85**, 1172–1178.
3 B. O'Regan and M. Gratzel, *Nature*, 1991, **353**, 737–740.
4 S. Ardo and G. J. Meyer, *Chem. Soc. Rev.*, 2009, **38**, 115–164.
5 A. Juris, V. Balzani, F. Barigelletti, S. Campagna, P. Belser and A. V. Zelewsky, *Coord. Chem. Rev.*, 1988, **84**, 85–277.
6 W. B. Heuer, H.-L. Xia, W. Ward, Z. Zhou, W. H. Pearson, M. A. Siegler, A. A. Narducci Sarjeant, M. Abrahamsson and G. J. Meyer, *Inorg. Chem.*, 2012, **51**, 3981–3988.
7 S. Altobello, R. Argazzi, S. Caramori, C. Contado, S. Da Fré, P. Rubino, C. Choné, G. Larramona and C. A. Bignozzi, *J. Am. Chem. Soc.*, 2005, **127**, 15342–15343.
8 E. A. M. Geary, L. J. Yellowlees, L. A. Jack, I. D. H. Oswald, S. Parsons, N. Hirata, J. R. Durrant and N. Robertson, *Inorg. Chem.*, 2005, **44**, 242–250.
9 G. M. Hasselmann and G. J. Meyer, *Z. Phys. Chem.*, 1999, **212**, 39–44.
10 S. Ferrere, *Chem. Mater.*, 2000, **12**, 1083–1089.
11 E. Baranoff, J.-H. Yum, M. Graetzel and M. K. Nazeeruddin, *J. Organomet. Chem.*, 2009, **694**, 2661–2670.
12 A. Yella, H. W. Lee, H. N. Tsao, C. Yi, A. K. Chandiran, M. K. Nazeeruddin, E. W. G. Diau, C. Y. Yeh, S. M. Zakeeruddin and M. Grätzel, *Science*, 2011, **334**, 629–634.
13 A. Mishra, M. K. R. Fischer and P. Büuerle, *Angew. Chem., Int. Ed.*, 2009, **48**, 2474–2499.
14 Z. Yao, M. Zhang, H. Wu, L. Yang, R. Li and P. Wang, *J. Am. Chem. Soc.*, 2015, **137**, 3799–3802.
15 J. B. Goodenough, *J. Phys. Chem.*, 1982, **86**, 3492–3492.
16 F. De Angelis, S. Fantacci, E. Mosconi, M. K. Nazeeruddin and M. Grätzel, *J. Phys. Chem. C*, 2011, **115**, 8825–8831.
17 A. Mishra, N. Pootrakulchote, M. K. R. Fischer, C. Klein, M. K. Nazeeruddin, S. M. Zakeeruddin, P. Bauerle and M. Gratzel, *Chem. Commun.*, 2009, 7146–7148.
18 M. Abrahamsson, P. G. Johansson, S. Ardo, A. Kopecky, E. Galoppini and G. J. Meyer, *J. Phys. Chem. Lett.*, 2010, 1725–1728.
19 P. Wang, C. Klein, J.-E. Moser, R. Humphry-Baker, N.-L. Cevey-Ha, R. Charvet, P. Comte, S. M. Zakeeruddin and M. Grätzel, *J. Phys. Chem. B*, 2004, **108**, 17553–17559.
20 I. Gillaizeau-Gauthier, F. Odobel, M. Alebbi, R. Argazzi, E. Costa, C. A. Bignozzi, P. Qu and G. J. Meyer, *Inorg. Chem.*, 2001, **40**, 6073–6079.
21 A. Buttner, S. Y. Brauchli, R. Vogt, E. C. Constable and C. E. Housecroft, *RSC Adv.*, 2016, **6**, 5205–5213.
22 S. Altobello, C. A. Bignozzi, S. Caramori, G. Larramona, S. Quici, G. Marzanni and R. Lakhmiri, *J. Photochem. Photobiol., A*, 2004, **166**, 91–98.
23 F. Odobel, L. Le Pleux, Y. Pellegrin and E. Blart, *Acc. Chem. Res.*, 2010, **43**, 1063–1071.
24 F. Odobel, Y. Pellegrin, E. A. Gibson, A. Hagfeldt, A. L. Smeigh and L. Hammarström, *Coord. Chem. Rev.*, 2012, **256**, 2414–2423.
25 J. Massin, S. Lyu, M. Pavone, A. B. Munoz-Garcia, B. Kauffmann, T. Toupance, M. Chavarot-Kerlidou, V. Artero and C. Olivier, *Dalton Trans.*, 2016, **45**, 12539–12547.
26 M. Gennari, F. Légalité, L. Zhang, Y. Pellegrin, E. Blart, J. Fortage, A. M. Brown, A. Deronzier, M.-N. Collomb, M. Boujtita, D. Jacquemin, L. Hammarström and F. Odobel, *J. Phys. Chem. Lett.*, 2014, **5**, 2254–2258.
27 C. J. Wood, K. C. D. Robson, P. I. P. Elliott, C. P. Berlinguette and E. A. Gibson, *RSC Adv.*, 2014, **4**, 5782–5791.
28 Z. Ji, G. Natu, Z. Huang, O. Kokhan, X. Zhang and Y. Wu, *J. Phys. Chem. C*, 2012, **116**, 16854–16863.
29 Y. Pellegrin, L. Le Pleux, E. Blart, A. Renaud, B. Chavillon, N. Szuwarski, M. Boujtita, L. Cario, S. Jobic, D. Jacquemin and F. Odobel, *J. Photochem. Photobiol., A*, 2011, **219**, 235–242.
30 A. Sinopoli, C. J. Wood, E. A. Gibson and P. I. P. Elliott, *Eur. J. Inorg. Chem.*, 2016, 2887–2890.
31 T. P. Lodge, *Macromol.*, 2009, **42**, 3827–3829.

32 E. Lim, *Int. J. Photoenergy*, 2013, **2013**, 607826, DOI: 10.1155/2013/607826.
33 D. Schweinfurth, K. I. Hardcastle and U. H. F. Bunz, *Chem. Commun.*, 2008, 2203–2205.
34 R. A. Fallahpour, *Helv. Chim. Acta*, 2000, **83**, 384–393.
35 B. S. Uppal, A. Zahid and P. I. P. Elliott, *Eur. J. Inorg. Chem.*, 2013, 2571–2579.
36 G. M. Hasselmann and G. J. Meyer, *J. Phys. Chem. B*, 1999, **103**, 7671–7675.
37 E. I. Mayo, K. Kilsa, T. Tirrell, P. I. Djurovich, A. Tamayo, M. E. Thompson, N. S. Lewis and H. B. Gray, *Photochem. Photobiol. Sci.*, 2006, **5**, 871–873.
38 T. N. Murakami, N. Koumura, M. Kimura and S. Mori, *Langmuir*, 2014, **30**, 2274–2279.
39 A. Nattestad, M. Ferguson, R. Kerr, Y.-B. Cheng and U. Bach, *Nanotechnology*, 2008, **19**, 295304.
40 M. K. Brennaman, R. J. Dillon, L. Alibabaei, M. K. Gish, C. J. Dares, D. L. Ashford, R. L. House, G. J. Meyer, J. M. Papanikolas and T. J. Meyer, *J. Am. Chem. Soc.*, 2016, **138**, 13085–13102.
41 K. K.-W. Lo and S. P.-Y. Li, *RSC Adv.*, 2014, **4**, 10560–10585.
42 M. Valiev, E. J. Bylaska, N. Govind, K. Kowalski, T. P. Straatsma, H. J. J. V. Dam, D. Wang, J. Nieplocha, E. Apra, T. L. Windus and W. d. Jong, *Comput. Phys. Commun.*, 2010, **181**, 1477–1660.
43 P. J. Stephens, F. J. Devlin, C. F. Chabalowski and M. J. Frisch, *J. Phys. Chem.*, 1994, **98**, 11623–11627.
44 A. D. Becke, *J. Chem. Phys.*, 1983, **98**, 5648–5652.
45 D. Andrae, U. Haussermann, M. Dolg, H. Stoll and H. Preuss, *Theor. Chim. Acta*, 1990, **77**, 123–141.
46 R. Krishnan, J. S. Binkley, R. Seeger and J. A. Pople, *J. Chem. Phys.*, 1980, **72**, 650–654.
47 E. Runge and E. K. U. Gross, *Phys. Rev. Lett.*, 1984, **52**, 997–1000.
48 A. Klamt and G. Schuurmann, *J. Chem. Soc., Perkin Trans. 2*, 1993, 799–805.